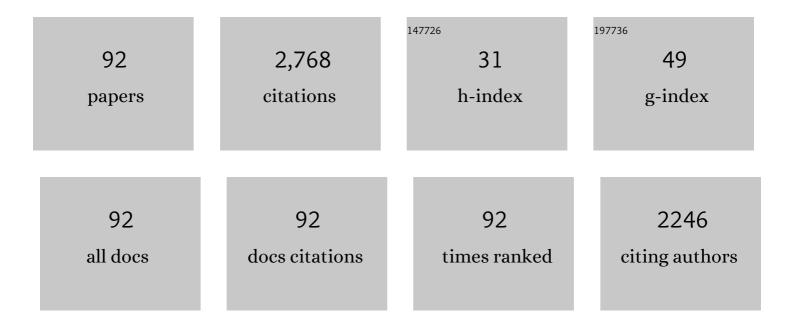
List of Publications by Year in descending order

Source: https://exaly.com/author-pdf/7922988/publications.pdf Version: 2024-02-01



#	Article	IF	CITATIONS
1	P-type doping of transition metal elements to optimize the thermoelectric properties of CuGaTe2. Chemical Engineering Journal, 2022, 427, 131807.	6.6	10
2	Decoupling of thermoelectric transport performance of Ag doped and Se alloyed tellurium induced by carrier mobility compensation. Journal of Materials Science and Technology, 2022, 101, 71-79.	5.6	2
3	Effects of solution cooling rate on the grain boundary and mechanical properties of GH4710 alloy. Materials Science & Engineering A: Structural Materials: Properties, Microstructure and Processing, 2022, 832, 142459.	2.6	8
4	Synergistically improving the thermoelectric and mechanical performance for p-type MnGe _{1â~<i>x</i>} Sb _{<i>x</i>} Te ₂ alloys. Physical Chemistry Chemical Physics, 2022, 24, 9247-9255.	1.3	4
5	Slab model studies of H2S adsorption/dissociation and diffusion on pristine FeS(001) surfaces and FeS(001) surfaces with pre-adsorbed X atoms (X = H, O, and S). Journal of Materials Research and Technology, 2022, 18, 1124-1136.	2.6	5
6	Achieving high thermoelectric performance through carrier concentration optimization and energy filtering in Cu3SbSe4-based materials. Journal of Materiomics, 2022, 8, 929-936.	2.8	7
7	Enhanced thermoelectric performance in n-type Mg3.2Sb1.5Bi0.5 doping with lanthanides at the Mg site. Journal of Materials Science and Technology, 2022, 127, 108-114.	5.6	3
8	Defect engineering synergistically modulates power factor and thermal conductivity of CuGaTe2 for ultra-high thermoelectric performance. Journal of Materials Science and Technology, 2022, 128, 213-220.	5.6	9
9	Influence of effective strain on the corrosion behavior of nickel-based GH4710 superalloy in chloride solutions. Corrosion Science, 2022, 204, 110386.	3.0	10
10	Significantly enhanced thermoelectric figure of merit of n-type Mg3Sb2-based Zintl phase compounds via co-doped of Mg and Sb site. Materials Today Physics, 2022, 26, 100721.	2.9	3
11	Adsorption and dissociation mechanism of hydrogen sulfide on layered FeS surfaces: A dispersion-corrected DFT study. Applied Surface Science, 2021, 537, 147905.	3.1	28
12	Realizing ultralow thermal conductivity in Cu3SbSe4 via all-scale phonon scattering by co-constructing multiscale heterostructure and IIIB element doping. Materials Today Energy, 2021, 19, 100620.	2.5	9
13	Effect of Impurity Atoms on the Adsorption/Dissociation of Hydrogen Sulfide and Hydrogen Diffusion on the Fe(100) Surface. ACS Omega, 2021, 6, 14701-14712.	1.6	5
14	Investigating the influence mechanism of hydrogen partial pressure on fracture toughness and fatigue life by in-situ hydrogen permeation. International Journal of Hydrogen Energy, 2021, 46, 20621-20629.	3.8	34
15	Exploring the Evolution Mechanism of Sulfur Vacancies by Investigating the Role of Vacancy Defects in the Interaction between H ₂ S and the FeS(001) Surface. ACS Omega, 2021, 6, 19212-19221.	1.6	6
16	Synergistic band convergence and defect engineering boost thermoelectric performance of SnTe. Journal of Materials Science and Technology, 2021, 86, 204-209.	5.6	27
17	New insights of the interaction of H2S with mackinawite FeS in a wet environment: An ab initio molecular dynamics study. International Journal of Hydrogen Energy, 2021, , .	3.8	2
18	Sn Doped FeNbSb Half-Heusler Compounds for Tuning Thermoelectric Performance. Journal of Electronic Materials, 2020, 49, 2862-2871.	1.0	8

#	Article	IF	CITATIONS
19	Ab initio molecular dynamics study of wet H2S adsorption and dissociation on Fe(100) surface. Journal of Molecular Liquids, 2020, 319, 114135.	2.3	11
20	Point defect engineering and machinability in n-type Mg3Sb2-based materials. Materials Today Physics, 2020, 15, 100269.	2.9	46
21	Hierarchical Structuring to Break the Amorphous Limit of Lattice Thermal Conductivity in High-Performance SnTe-Based Thermoelectrics. ACS Applied Materials & Interfaces, 2020, 12, 36370-36379.	4.0	20
22	Realizing High Thermoelectric Performance in the ZnTe-Alloyed CuGaTe2 through Band Engineering. ACS Applied Energy Materials, 2020, 3, 12400-12406.	2.5	8
23	Crowding-out effect strategy using AgCl for realizing a super low lattice thermal conductivity of SnTe. Sustainable Materials and Technologies, 2020, 25, e00183.	1.7	6
24	A novel antiferromagnetic semiconductor hidden in pyrite. Computational Materials Science, 2020, 183, 109852.	1.4	7
25	Synergistic modulation of power factor and thermal conductivity in Cu3SbSe4 towards high thermoelectric performance. Nano Energy, 2020, 71, 104658.	8.2	36
26	Synergistically improving thermoelectric and mechanical properties of Ge0.94Bi0.06Te through dispersing nano-SiC. Scripta Materialia, 2020, 183, 22-27.	2.6	29
27	The effects of double notches on the mechanical properties of a high-strength pipeline steel under hydrogen atmosphere. International Journal of Hydrogen Energy, 2020, 45, 23134-23141.	3.8	8
28	Enhanced thermoelectric performance of In and Se co-doped GeTe compounds. Journal of Materials Research and Technology, 2020, 9, 4106-4113.	2.6	12
29	Band Engineering and Thermoelectric Performance Optimization of p-Type GeTe-Based Alloys through Ti/Sb Co-Doping. Journal of Physical Chemistry C, 2020, 124, 5583-5590.	1.5	16
30	Band Engineering for Realizing Large Effective Mass in Cu ₃ SbSe ₄ by Sn/La Codoping. Journal of Physical Chemistry C, 2020, 124, 10336-10343.	1.5	22
31	The dependence of anti-corrosion behaviors of iron sulfide films on different reactants. International Journal of Hydrogen Energy, 2020, 45, 17548-17556.	3.8	6
32	Defect Chemistry for N-Type Doping of Mg ₃ Sb ₂ -Based Thermoelectric Materials. Journal of Physical Chemistry C, 2019, 123, 20781-20788.	1.5	23
33	Hydrogen-Assisted Crack Growth in the Heat-Affected Zone of X80 Steels during in Situ Hydrogen Charging. Materials, 2019, 12, 2575.	1.3	9
34	Improvement of thermoelectric properties of Cu3SbSe4 hierarchical with in-situ second phase synthesized by microwave-assisted solvothermal method. Journal of Alloys and Compounds, 2019, 806, 676-682.	2.8	15
35	The manipulation of substitutional defects for realizing high thermoelectric performance in Mg ₃ Sb ₂ -based Zintl compounds. Journal of Materials Chemistry A, 2019, 7, 19316-19323.	5.2	45
36	Effects of shot peening on tensile properties and fatigue behavior of X80 pipeline steel in hydrogen environment. International Journal of Fatigue, 2019, 129, 105235.	2.8	12

#	Article	IF	CITATIONS
37	Cu/Sb Codoping for Tuning Carrier Concentration and Thermoelectric Performance of GeTe-Based Alloys with Ultralow Lattice Thermal Conductivity. ACS Applied Energy Materials, 2019, 2, 2596-2603.	2.5	45
38	Synergistic action of hydrogen gas and weld defects on fracture toughness of X80 pipeline steel. International Journal of Fatigue, 2019, 120, 23-32.	2.8	27
39	Computational prediction of high thermoelectric performance in p-type CuGaTe2 with a first-principles study. Computational Materials Science, 2019, 158, 369-375.	1.4	15
40	Effect of vacancy on adsorption/dissociation and diffusion of H2S on Fe(1 0 0) surfaces: A density functional theory study. Applied Surface Science, 2019, 465, 833-845.	3.1	27
41	Self-assembled 3D flower-like hierarchical Ti-doped Cu3SbSe4 microspheres with ultralow thermal conductivity and high zT. Nano Energy, 2018, 49, 221-229.	8.2	45
42	Computational prediction of a high <i>ZT</i> of n-type Mg ₃ Sb ₂ -based compounds with isotropic thermoelectric conduction performance. Physical Chemistry Chemical Physics, 2018, 20, 7686-7693.	1.3	55
43	Roles of carbon dioxide and steam on the hydrogen embrittlement of 3Cr tube steel in synthetic natural gas environment. Corrosion Engineering Science and Technology, 2018, 53, 1-10.	0.7	5
44	Designing high-performance n-type Mg ₃ Sb ₂ -based thermoelectric materials through forming solid solutions and biaxial strain. Journal of Materials Chemistry A, 2018, 6, 20454-20462.	5.2	32
45	Vapor-deposited iron sulfide films as a novel hydrogen permeation barrier for steel: Deposition condition, defect effect, and hydrogen diffusion mechanism. International Journal of Hydrogen Energy, 2018, 43, 15564-15574.	3.8	21
46	Investigation of Hydrogen Embrittlement Susceptibility of X80 Weld Joints by Thermal Simulation. Journal of Materials Engineering and Performance, 2018, 27, 2513-2523.	1.2	1
47	Review of recent progress in the study of corrosion products of steels in a hydrogen sulphide environment. Corrosion Science, 2018, 139, 124-140.	3.0	119
48	Computational prediction of high thermoelectric performance in p-type half-Heusler compounds with low band effective mass. Physical Chemistry Chemical Physics, 2017, 19, 4411-4417.	1.3	88
49	Simultaneous optimization of electrical and thermal transport properties of Bi0.5Sb1.5Te3 thermoelectric alloy by twin boundary engineering. Nano Energy, 2017, 37, 203-213.	8.2	164
50	Synergistic action of hydrogen and stress concentration on the fatigue properties of X80 pipeline steel. Materials Science & Engineering A: Structural Materials: Properties, Microstructure and Processing, 2017, 700, 321-330.	2.6	35
51	Influence of hydrogen pressure on fatigue properties of X80 pipeline steel. International Journal of Hydrogen Energy, 2017, 42, 15669-15678.	3.8	44
52	First-principles calculations of the structural, elastic and thermodynamic properties of mackinawite (FeS) and pyrite (FeS 2). Physica B: Condensed Matter, 2017, 525, 119-126.	1.3	28
53	Thermoelectric Performance of Se/Cd Codoped SnTe via Microwave Solvothermal Method. ACS Applied Materials & Interfaces, 2017, 9, 22612-22619.	4.0	51
54	Validity of Rigid-Band Approximation in the Study of Thermoelectric Properties of p-Type FeNbSb-Based Half-Heusler Compounds. Journal of Electronic Materials, 2017, 46, 3030-3035.	1.0	20

#	Article	IF	CITATIONS
55	Enhanced Electronic Transport Properties of Se-Doped SnTe1â^'xSex Nanoparticles by Microwave-Assisted Solvothermal Method. Journal of Electronic Materials, 2017, 46, 2847-2853.	1.0	9
56	Influence of H2S interaction with prestrain on the mechanical properties of high-strength X80 steel. International Journal of Hydrogen Energy, 2016, 41, 10412-10420.	3.8	46
57	Enhancing thermoelectric performance through one-pot solution phase synthesis of Bi2S3 nanobundles. Materials Letters, 2016, 185, 67-71.	1.3	19
58	Systhesizing SnTe nanocrystals leading to thermoelectric performance enhancement via an ultra-fast microwave hydrothermal method. Nano Energy, 2016, 28, 78-86.	8.2	79
59	Effect of Amorphous FeS Semiconductor on the Corrosion Behavior of Pipe Steel in H ₂ S-Containing Environments. Industrial & Engineering Chemistry Research, 2016, 55, 10932-10940.	1.8	30
60	An efficient precursor to synthesize various FeS2nanostructures via a simple hydrothermal synthesis method. CrystEngComm, 2016, 18, 6262-6271.	1.3	43
61	Electronic structure and thermoelectric properties of p-type half-Heusler compound NbFeSb: a first-principles study. RSC Advances, 2016, 6, 10507-10512.	1.7	42
62	Effect of H 2 S/CO 2 partial pressure ratio on theÂtensile properties of X80 pipeline steel. International Journal of Hydrogen Energy, 2015, 40, 11925-11930.	3.8	42
63	Tensile and impact properties of X70 pipeline steel exposed to wet H 2 S environments. International Journal of Hydrogen Energy, 2015, 40, 11514-11521.	3.8	29
64	Initiation and developmental stages of steel corrosion in wet H2S environments. Corrosion Science, 2015, 93, 109-119.	3.0	116
65	High-Yield Synthesis, Controllable Evolution, and Thermoelectric Properties of Te/Bi2Te3 Heterostructure Nanostrings. Journal of Electronic Materials, 2015, 44, 2061-2067.	1.0	10
66	Microwave-assisted synthesis of pyrite FeS ₂ microspheres with strong absorption performance. RSC Advances, 2015, 5, 65575-65582.	1.7	25
67	Rational design and controlled synthesis of Te/Bi2Te3 heterostructure nanostring composites. Journal of Crystal Growth, 2015, 421, 13-18.	0.7	12
68	Effect of H 2 /CO 2 partial pressure ratio on the tensile properties of X80 pipeline steel in the absence and presence of water. International Journal of Hydrogen Energy, 2015, 40, 11917-11924.	3.8	11
69	Electrochemical characteristics of the early corrosion stages of API X52 steel exposed to H2S environments. Materials Chemistry and Physics, 2015, 149-150, 295-301.	2.0	50
70	Comparison of tensile and impact behavior of carbon steel in H2S environments. Materials & Design, 2014, 58, 234-241.	5.1	28
71	Single-crystalline Bi2Te3 nanosheets with uniform morphology via a simple, efficient, and high-yield microwave-assisted synthesis. Journal of Crystal Growth, 2014, 406, 104-110.	0.7	18
72	Effects of environmental conditions on hydrogen permeation of X52 pipeline steel exposed to high H2S-containing solutions. Corrosion Science, 2014, 89, 30-37.	3.0	53

#	Article	IF	CITATIONS
73	Investigation of the Iron–Sulfide Phase Transformation in Nanoscale. Crystal Growth and Design, 2014, 14, 4295-4302.	1.4	36
74	Investigations of the diverse corrosion products on steel in a hydrogen sulfide environment. Corrosion Science, 2014, 87, 397-406.	3.0	76
75	Rational design, high-yield synthesis, and low thermal conductivity of Te/Bi 2 Te 3 core/shell heterostructure nanotube composites. Journal of Alloys and Compounds, 2014, 617, 247-252.	2.8	11
76	Dependence of the abnormal protective property on the corrosion product film formed on H2S-adjacent API-X52 pipeline steel. International Journal of Hydrogen Energy, 2014, 39, 13919-13925.	3.8	34
77	Effect of H2S partial pressure on the tensile properties of A350LF2 steel in the absence and presence of pre-immersion. Materials Science & Engineering A: Structural Materials: Properties, Microstructure and Processing, 2014, 609, 161-167.	2.6	12
78	Controlled synthesis of tellurium nanowires and nanotubes via a facile, efficient, and relatively green solution phase method. Journal of Materials Chemistry A, 2013, 1, 15046.	5.2	55
79	Effect of immersion time on the hydrogen content and tensile properties of A350LF2 steel exposed to hydrogen sulphide environments. Corrosion Science, 2013, 69, 164-174.	3.0	43
80	Mechanism of (Mg,Al,Ca)-oxide inclusion-induced pitting corrosion in 316L stainless steel exposed to sulphur environments containing chloride ion. Corrosion Science, 2013, 67, 20-31.	3.0	192
81	The effect of the partial pressure of H2S on the permeation of hydrogen in low carbon pipeline steel. Corrosion Science, 2013, 67, 184-192.	3.0	106
82	Effect of hydrogen and inclusions on the tensile properties and fracture behaviour of A350LF2 steels after exposure to wet H2S environments. Corrosion Science, 2012, 60, 59-68.	3.0	49
83	First-principles study of hydrogen diffusion mechanism in Cr2O3. Science China Technological Sciences, 2011, 54, 88-94.	2.0	20
84	Corrosion Electrochemical Characteristics of the Passive Films Formed on Inconel 718 Alloy in the Environments Containing High H ₂ S and CO ₂ Partial Pressures. Nanoscience and Nanotechnology Letters, 2011, 3, 204-208.	0.4	5
85	The non-linear fitting method to analyze the measured M–S plots of bipolar passive films. Electrochimica Acta, 2010, 55, 2498-2504.	2.6	53
86	Investigation of the degradation of smooth SiGe epitaxial layer on Si substrate. Microelectronics Journal, 2008, 39, 53-56.	1.1	2
87	The structural deformations in the Si/SiGe system induced by thermal annealing. Journal of Materials Science, 2007, 42, 5312-5317.	1.7	7
88	Interdiffusion at Si/SiGe interface analyzed by high-resolution X-ray diffraction. Thin Solid Films, 2006, 508, 156-159.	0.8	12
89	Reaction synthesis and formation mechanism of barium hexaboride. Materials Letters, 2003, 57, 1330-1333.	1.3	9
90	Icosahedral phase in rapidly solidified Al–Fe–Ce alloy. Materials Science & Engineering A: Structural Materials: Properties, Microstructure and Processing, 2002, 323, 226-231.	2.6	15

#	Article	IF	CITATIONS
91	Synthesis of Calcium Hexaboride Powder via the Reaction of Calcium Carbonate with Boron Carbide and Carbon. Journal of the American Ceramic Society, 2001, 84, 2725-2727.	1.9	35
92	Theoretical Study on Thermoelectric Performance of N‶ype Mg ₃ (Sb,Bi) ₂ Single Crystal for Cooling or Power Generation. Advanced Theory and Simulations, 0, , 2200049.	1.3	1